

Improving Extrinsic between RADAR and LIDAR using Learning

Peng Jiang

*J. Mike Walker '66 Dept. of Mechanical Engineering
Texas A&M University
College Station, USA
maskjp@tamu.edu*

Srikanth Saripalli

*J. Mike Walker '66 Dept. of Mechanical Engineering
Texas A&M University
College Station, USA
ssaripalli@tamu.edu*

Abstract—LIDAR and RADAR are two commonly used sensors in autonomous driving systems. The extrinsic calibration between the two is crucial for effective sensor fusion. The challenge arises due to the low accuracy and sparse information in RADAR measurements. This paper presents a novel solution for 3D RADAR-LIDAR calibration in autonomous systems. The method employs simple targets to generate data, including correspondence registration and a one-step optimization algorithm. The optimization aims to minimize the reprojection error while utilizing a small multi-layer perception (MLP) to perform regression on the return energy of the sensor around the targets. The proposed approach uses a deep learning framework such as PyTorch and can be optimized through gradient descent. The experiment uses a 360-degree Ouster-128 LIDAR and a 360-degree Navtech RADAR, providing raw measurements. The results validate the effectiveness of the proposed method in achieving improved estimates of extrinsic calibration parameters.

Index Terms—RADAR, LIDAR, Calibration, Neural Network, NeRF

I. INTRODUCTION

With the advancement of autonomous vehicle technology, there is an increasing need for effective solutions in adverse weather conditions, such as rain and snow. While CAMERA and LIDAR sensors have proven successful under normal conditions, inclement weather can significantly affect their performance. RADAR sensors, like those produced by Navtech [1], offer a promising alternative. With a longer wavelength, RADAR sensors are less impacted by small particles like dust, fog, rain, or snow that can impair the performance of CAMERA and LIDAR. Additionally, RADAR has a longer detection range and the ability to penetrate materials, enabling the detection of objects that are beyond the line of sight of LIDAR sensors. These features make RADAR ideal for use in adverse weather conditions.

The publication of the Oxford RADAR RobotCar Dataset [1] in 2020 has provided a valuable resource for researchers, containing a rich collection of LIDAR, CAMERA, and RADAR data. This dataset has been instrumental in advancing autonomous vehicle research and has led to notable progress in fields such as odometry [1]–[4], place recognition [5], [6], and semantic segmentation [7]–[10]. Other datasets like [11]–[14] have also been made accessible to researchers, further fueling the development of RADAR research. We expect RADAR and its integration with other sensors to become a growing area of

research and application in the future, with great advancements driven by the availability of large amounts of public data.

While RADAR sensors have the potential to provide robust performance in inclement weather, they also have a coarser spatial resolution and higher noise compared to LIDAR sensors, making the task of calibrating them challenging. Extrinsic calibration between RADAR and other sensors has received relatively less attention compared to the calibration between LIDAR and CAMERA sensors [11], [15]–[18].

The extrinsic 6-DoF calibration between LIDAR and RADAR sensors can be difficult due to the limited resolution and information loss in the third dimension of RADAR measurements. Previous methods, such as [19], utilized curve models to model the relationship between elevation and RADAR cross-section (RCS). However, these models have limitations as they only consider a subset of data and do not account for various factors that impact the RADAR return signal, such as shape, material, direction, and the RADAR's power and frequency. Recent advancements in neural networks, such as the Neural Radiance Field (NeRF) model [20], demonstrate the ability to model complex relationships between sensors, poses, and scenes, including scene geometry. These models can learn to represent a scene using images from various views and estimate the pose during the training process [21]. In this paper, we present a method to calibrate LIDAR and RADAR by using a small Multi-Layer Perceptron (MLP) to model the target as a collection of RADAR return energy. The model is trained to learn the correlation between the RADAR sensor pose relative to the target and the return energy, allowing it to be used for calibration. This is treated as a regression problem. Along with the regression loss, we also use reprojection loss and a ray pass loss to achieve calibration. The details of these losses will be described in III-C.

II. RELATED WORKS

A. Multisensor Calibration

In the calibration of RADAR and other sensors, two primary challenges exist: (1) recovering the missing third-dimension information from RADAR and other sensors, and (2) ensuring that reflectors are visible to all sensors. Traditional methods have addressed these issues in various ways. For example, [22] proposed a 3D reconstruction method based on sensor

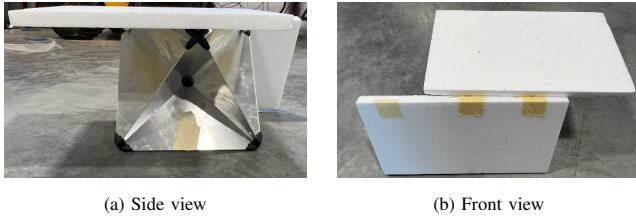


Fig. 1. Aluminum octahedral RADAR reflector front with two sides covered by two polystyrene foams

geometry and a calibration facility using a Luneburg lens and differently-colored corner reflectors. [23] designed a compact target and proposed two-step optimizations for 6-DOF calibration between RADAR and LIDAR. Subsequently, [19] added chequerboard patterns to enable calibration between RADAR, LIDAR, and CAMERA. [24] utilized a styrofoam board with four circular holes and a corner reflector for sparse LIDAR beam detection. More recent tools like *radar_to_lidar_calib* [25] and *OpenCalib* [26] have also emerged, offering calibration capabilities for multiple sensor types without targets. Our novel approach distinguishes itself from these existing methods by utilizing a more comprehensive representation of the target, rather than only considering data with the strongest return energy. We achieve this by training a small neural network to represent the target, which allows our method to account for both the detected target center, characterized by high return energy, and the data from the surrounding neighborhood. This innovative approach leads to a more accurate and nuanced calibration process, ensuring enhanced performance in multi-sensor systems.

B. RADAR and Neural Network

Deep learning has demonstrated its effectiveness in various applications, including autonomous driving. While CAMERA and LIDAR have benefited from extensive research, the application of deep learning to RADAR remains under-explored, as evidenced by the limited literature [11]. Notable works on CAMERA and LIDAR calibration using deep learning, such as [15]–[18], have employed supervised or unsupervised approaches, but similar studies for RADAR and other sensor calibrations are still lacking. These methods leverage neural networks to identify correlations between modalities and learn common features, either guided by ground truth or an unsupervised loss. A promising future direction could involve unsupervised metric feature learning techniques, such as [2], [3], for discovering shared features between RADAR and other modalities, as demonstrated in [27]. Implicit neural representations have recently gained popularity in representing scenes for images and 3D point clouds. Gradient descent allows neural networks to learn color and geometry information from image data [20] or point cloud data [28], with or without pose information. However, to the best of our knowledge, this approach has not yet been applied to RADAR data. Our work stands out by exploring the untapped potential of deep learning

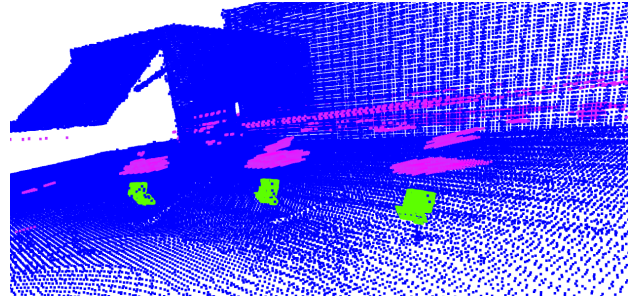


Fig. 2. Registered LIDAR Point Cloud (blue), Filtered RADAR measurements (Purple), Extracted Target Point Cloud (green)

in RADAR calibration, addressing the gap in existing research and offering a novel contribution to the field.

III. METHOD

A. Calibration Target Design

Calibrating both LIDAR and RADAR requires a target that is visible to both sensors. For RADAR, it is desirable to have a target with a high RADAR Cross-Section (RCS) to improve the detection rates. Marine aluminum RADAR reflectors (see Fig. 1 (a)), which are cheap and readily available, can be used for this purpose, but they can affect the LIDAR measurements. Furthermore, their small size makes them difficult to detect by LIDAR. To overcome this, we use two polystyrene foams to cover two sides of the reflector and construct a non-symmetrical shape as see Fig. 1 (b), which has a larger visible area for LIDAR, making it easier to register and determine the reflector's position in the scene, which will be used for calibration.

B. Data Collection

To guarantee accurate and undistorted data from both LIDAR and RADAR sensors, we leverage velocity information obtained from the Inertial Measurement Unit (IMU) sensor to identify static frames in LIDAR and RADAR data. We used the FPFH feature [29] and RANSAC global registration to register all the static LIDAR frames together, resulting in an initial pose of all the LIDAR data in the scene. We then refined the pose of each LIDAR frame using the Iterative Closest Point (ICP) algorithm to generate a dense LIDAR point cloud, which was then utilized for target detection to prevent any incomplete frames. By collecting data from multiple robot movements, we obtained each LIDAR frame's position within the registered point cloud, thus eliminating the need for target extraction for each frame. For the RADAR target extraction, we first filtered out most of the raw RADAR by setting a threshold. Then we used raw LIDAR and RADAR transformation to get the raw data target measurement, which was obtained by manually measuring. We defined the target center as the first measurement in the RADAR data. The data collection and pre-processing results is shown in Fig.2.

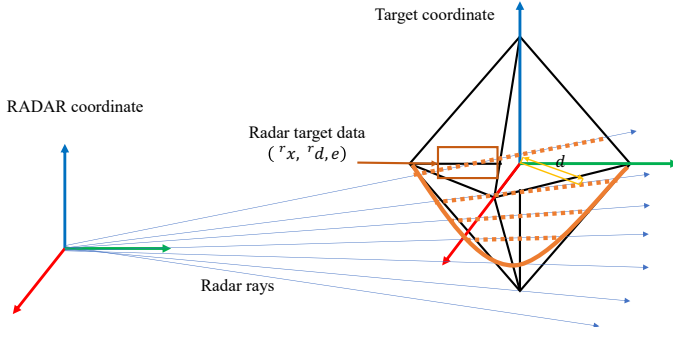


Fig. 3. Sample the RADAR measurement data $({}^r\mathbf{x}_i, {}^r\mathbf{d}_i, e_i)$ around the target centers; Compute the data distance d between the LIDAR target center and the RADAR target center

C. Optimization

We develop our calibration method using a gradient descent optimization framework implemented with PyTorch. Our objectives for the calibration are three-fold: 1) minimizing the reprojection error, 2) reducing the regression error of an MLP, and 3) minimizing the ray pass loss, which considers whether a ray passes through the target or not. The transformation matrix T between the LIDAR and RADAR sensors can be represented in many ways. While optimizing, the rotation matrix $R(\mathbf{w})$ was represented as axis-angle representation \mathbf{w} ($\mathfrak{so}(3) \rightarrow \text{SO}(3)$). While evaluation, we represent the rotation using Euler angles $\boldsymbol{\theta} = [\theta_x, \theta_y, \theta_z]$. The translation is represented by three variables $\mathbf{t} = [t_x, t_y, t_z]$.

1) *Reprojection Loss*: To compute reprojection loss, we first convert the LIDAR target center point ${}^l\mathbf{x}_{l,i}$ from the LIDAR sensor coordinate to the RADAR sensor coordinate using the following equation:

$${}^r\mathbf{x}_{l,i} = {}^r_l R \cdot {}^l\mathbf{x}_{l,i} + {}^r_l \mathbf{t} \quad (1)$$

Where ${}^r_l R$ is the rotation matrix and ${}^r_l \mathbf{t}$ is the translation vector. Next, the point ${}^r\mathbf{x}_{l,i}$ is converted to spherical coordinate ${}^r\mathbf{s}_{l,i} = [{}^r r_{l,i}, {}^r \theta_{l,i}, {}^r z_{l,i}]$. The RADAR measurement ${}^r\mathbf{s}_{r,i} = [{}^r r_{r,i}, {}^r \theta_{r,i}, -]$ is assumed to be the ground truth. The absolute differences loss (L_1) is applied to the azimuth angle and radial distance between the transformed LIDAR target center data and the RADAR measurement.

$$l_{rep} = w_r L_1({}^r r_r, {}^r r_l) + w_\theta L_1({}^r \theta_r, {}^r \theta_l) \quad (2)$$

where w_θ and w_r are two weights that can be set manually to adjust the optimization direction and balance the relative importance of radial distance and azimuth angle, due to their differing value scales.

2) *Regression Loss*: Getting a 6 DoF calibration between LIDAR and RADAR is challenging due to the missing 3D information in RADAR measurement. However, as shown in [19], the RCS is correlated with the target's 3D position in the RADAR coordinate, leading to the modeling of the relationship between RCS and target position as a curve model in the paper. Inspired by this work and recent advancements in NeRF, we use a small Multi-Layer Perceptron (MLP) to model

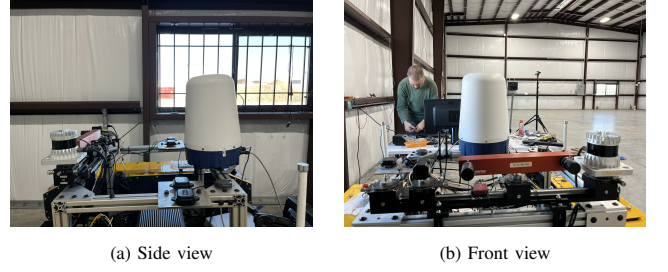


Fig. 4. Clearpath Warthog with one Ouster OS1 128 Channel LIDAR and one Navtech CIR-DEV RADAR

the relationship between the RADAR sensor pose relative to the target and the return energy. Rather than solely relying on the target center to model the relationship, we also incorporate the neighborhood data surrounding the target centers for a more comprehensive representation. See. Fig.3, we sample the RADAR measurement data around the target centers and represent the data as $({}^r\mathbf{x}_{r,i}, {}^r\mathbf{d}_{r,i}, e_i)$, where ${}^r\mathbf{x}_{r,i}$ denote the position of the RADAR data in RADAR coordinate, ${}^r\mathbf{d}_{r,i}$ represent the ray direction from the RADAR sensor origin to the measurement, and e_i represent the return energy, which is raw data value of the Navtech RADAR.

In the optimization process, we transform the RADAR measurement $({}^r\mathbf{x}_{r,i}, {}^r\mathbf{d}_{r,i}, e_i)$ from the RADAR coordinate to the local target coordinate based on the current estimated RADAR-LIDAR extrinsic calibration ${}^w_r T$ and the target pose ${}^w T$ in the scene which can be obtained during the data collection steps described in III-B. After the transformation, we got data $({}^t\mathbf{x}_{r,i}, {}^t\mathbf{d}_{r,i}, e_i)$ in the target local coordinate. Based on [20] and experiment, we use Eq.3 to apply position encoding to each of the three coordinate values in the direction ${}^t\mathbf{d}_{r,i}$ and position ${}^t\mathbf{x}_{r,i}$ separately. Eq.3 is a mapping from \mathbb{R} into a higher dimensional space \mathbb{R}^{2L} . Positional encoding facilitates the network to optimize parameters by easily mapping input to higher-dimensional space. [20] showed that using a high-frequency function for mapping original input enables better fitting of data that contains high-frequency variation.

$$\begin{aligned} P(x, 2i) &= \sin(2^i \pi x) \\ P(x, 2i + 1) &= \cos(2^i \pi x) \end{aligned} \quad (3)$$

We use the encoded direction $P({}^t\mathbf{d}_{r,i})$ and position $P({}^t\mathbf{x}_{r,i})$ as the input of the MLP and predict the corresponding return energy \hat{e}_i .

$$\hat{e}_i = \text{MLP}(P({}^t\mathbf{x}_{r,i}), P({}^t\mathbf{d}_{r,i})) \quad (4)$$

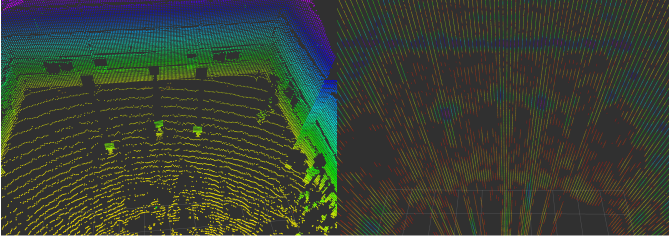
During optimization, we minimize the absolute difference (L_1 loss) between the ground truth value e_i and the predictions \hat{e}_i

$$l_{mlp} = L_1(\hat{e}_i, e_i) \quad (5)$$

3) *Ray-pass Loss*: To ensure that our optimization results align with the properties of the sensors, we added a ray pass loss to optimization objectives. The high return energy of RADAR target measurement should be the result of a ray passing through the target from the RADAR sensor origin.



(a) Sensors and Targets Setup for Data Collection



(b) Raw LIDAR data

(c) Raw RADAR data

Fig. 5. Experiment settings: Three targets with fixed positions form a scene, and the robot drives around the targets.

To simplify, we modeled the target as a ball rather than an octahedron. The loss is defined as in Equation 6, where d is the distance between the ray and the center of the target in the target coordinate system, and r is the radius of the circumscribed sphere. If the distance is greater than the radius, it indicates that the ray does not pass through the target, and the difference between the distance and radius is used as the penalty. If the distance is smaller than the radius, the penalty is set to zero.

$$l_{ray} = \max(0, d_i - r) \quad (6)$$

4) *Total Losses*: The overall optimization objective is:

$$l = w_{rep}l_{rep} + w_{mlp}l_{mlp} + w_{ray}l_{ray} \quad (7)$$

where the w_{rep} , w_{mlp} and w_{ray} are weights for each loss.

IV. EXPERIMENTS

A. Sensors and Experiment Setting

The experiment involved a Clearpath Warthog mobile robot equipped with an Ouster OS1 3D LIDAR and a Navtech CIR-DE RADAR, as depicted in Fig. 5. The LIDAR has 128 channels and 2048 points per channel, with an 45 degrees vertical field of view (FoV) and operates at 10 Hz. The RADAR has a range resolution of 0.044m and azimuth resolution of 0.9 degrees, with an 1.8 degrees vertical field of view (FoV) and works a 4 Hz. Both sensors have 360 degrees horizontal field of view (FoV). The sensor setup is shown in Figure 4. A 3D-printed wedge was attached to the bottom of the RADAR with an incline of around three degrees.

The experiment used three targets, and the robot was positioned at different locations to collect data, as shown in Fig. 5. The experiment was conducted outdoors, and five different target settings were used. After the data processing

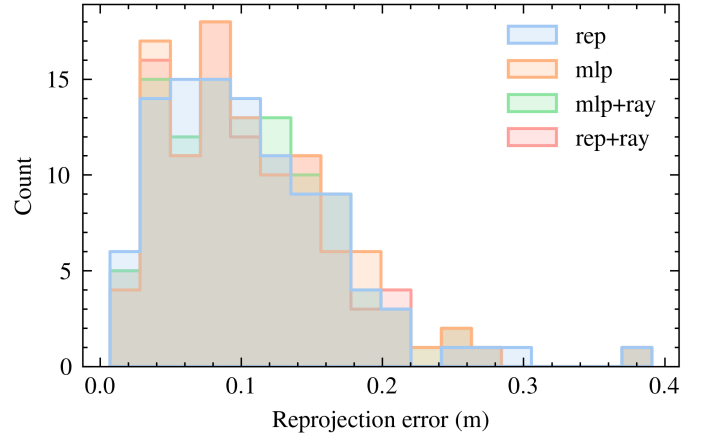


Fig. 6. Histogram of reprojection errors for RADAR-LIDAR calibration using different loss configuration

steps described in III-B, 104 paired RADAR-LIDAR data were collected.

B. Implementation

Our extrinsic calibration algorithm was implemented using the PyTorch framework and optimized using the Adam optimizer [30]. The MLP consisted of four linear layers, each with a hidden size of 128 and using the ReLU activation function. A learning rate of 0.005 was applied to the network, while the learning rates for the rotation and translation parameters were set to 0.005 and 0.001, respectively. During the experiment, the weights for the reprojection error, regression, and ray-pass losses were set to 1000, 1000, and 100, respectively. To compute the regression loss, we sampled data around the estimated RADAR target center within a radius of 0.6 meters.

C. Results

To evaluate the quality of the calibration results, we conducted experiments on a real-world dataset with different loss function configurations: including only the reprojection error loss (*rep*), the reprojection error loss and regression loss (*mlp*), the reprojection error loss, regression loss, and ray-pass loss (*mlp+ray*) and the reprojection error loss and ray-pass loss (*rep+ray*). Table I presents the initial calibration parameters obtained manually and the results of calibrations

TABLE I
RADAR-LIDAR CALIBRATION RESULTS

Loss	θ_x	θ_y	θ_z	t_x	t_y	t_z
initial	0.00	0.00	0.00	0.50	-0.25	0.05
rep	0.97	6.97	1.17	0.57	-0.26	0.04
mlp	0.26	2.04	1.01	0.57	-0.25	0.05
mlp+ray	-0.14	2.63	1.05	0.56	-0.26	-0.03
rep+ray	0.08	3.35	1.07	0.57	-0.26	0.01

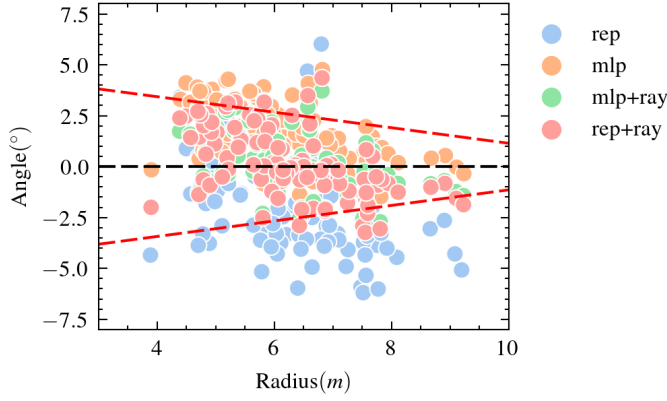


Fig. 7. LIDAR target centers distribution in the RADAR coordinate. The x-axis represents the radial distance between the target center and the RADAR origin, the y-axis represents the angle between the RADAR x-y plane and the target centers.

using different optimization objectives. The results demonstrate differences, particularly in θ_x and θ_y , and t_z , due to the limitations of the RADAR measurement. However, as previously mentioned, we intentionally introduced a three-degree wedge while installing RADAR sensors. As shown in Table I, all calibration results reflect this. We used the reprojection error in the RADAR coordinate as the evaluation metric, and Fig. 6 shows the distribution of the reprojection error. Despite the differences, all four settings have similar reprojection error distributions, which does not necessarily indicate which calibration results are better.

To further evaluate the quality of the calibration results, we examine the relationship between the target and RADAR ray. The RADAR ray from the sensor origin to the RADAR target center must hit the target and return the energy, as indicated by the high return energy. Fig. 7 displays the distribution of the LIDAR target centers in the RADAR coordinate after projection using the calibration results. The x-axis represents the radial distance between the LIDAR target center and the RADAR origin. In contrast, the y-axis represents the angle between the RADAR x-y plane and the LIDAR target centers. The two red dashed lines indicate the boundaries where the RADAR ray can hit the target at different distances based on the physical size of the target. From Fig. 7, we observe that the calibration results that only use the reprojection error loss have many points outside the boundary, which is not physically correct. On the other hand, the calibration results of *mlp+ray* and *rep+ray* have most of the projected points within the boundaries. The *mlp* also has most of the points within or close to the boundary, which implies that the objective function is effective. In order to evaluate the robustness of our method, we conducted a Monte Carlo analysis by randomly subsampling our dataset to 50% of its original size and ran 100 iterations of optimization on different subsampled datasets. The results are presented as boxplots in Fig. 8. As predicted and in line with previous studies [19], [23], the parameters t_x , t_y , and θ_z that are well-represented by the RADAR measurements

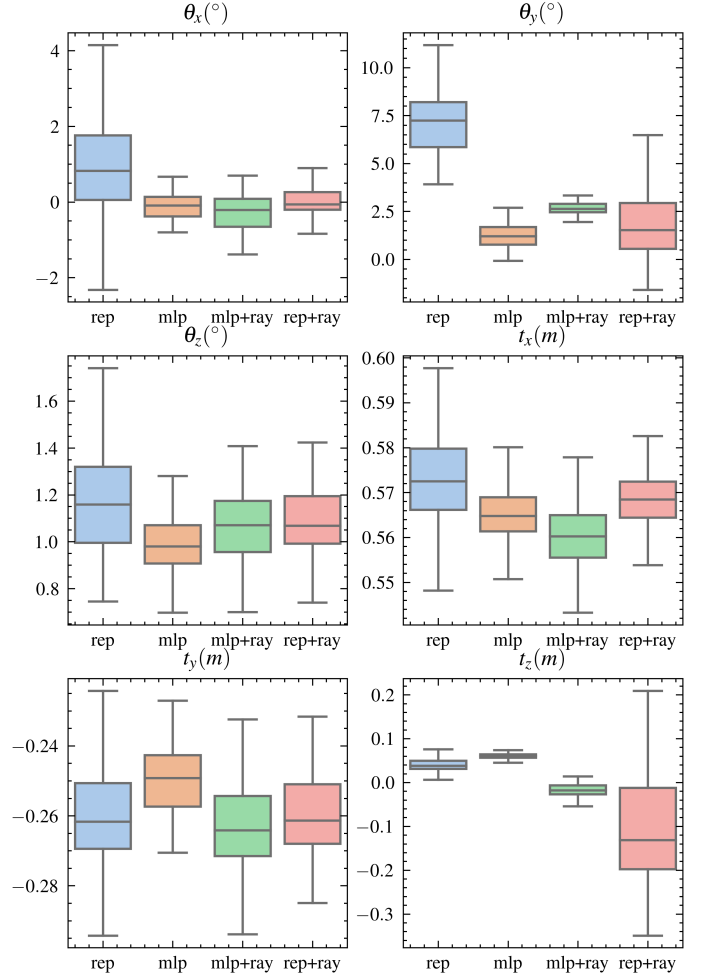


Fig. 8. Monte Carlo analysis results for RADAR-LIDAR calibration using different loss configurations

exhibit lower variance compared to the other parameters. In contrast, the parameters t_z , θ_x , and θ_y show larger variance. The results from the *rep+ray* experiment display the highest variance in z , indicating that the ray-pass loss function is highly sensitive to the amount of data. By incorporating the regression loss, which utilizes both reprojection error and the relationship between the return energy and the position of the target center's surroundings, the variance is reduced compared to only using reprojection error and ray-pass, even with fewer data points. Finally, Fig. 10 demonstrates that the use of positional encoding results in smaller errors in regression. Several examples of the regression are illustrated in Fig. 9.

V. CONCLUSION

In this study, we presented a novel extrinsic 6-DoF calibration method for a RADAR-LIDAR system. Our method used a specially designed calibration target that allowed both sensors to accurately detect and locate the target within their respective operating parameters. The calibration process involved three optimization objectives: reprojection error, regression error, and ray-pass loss. The proposed method was implemented

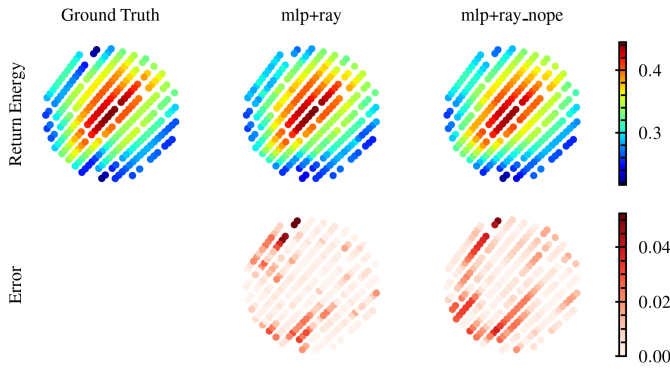


Fig. 9. Regression results from MLP

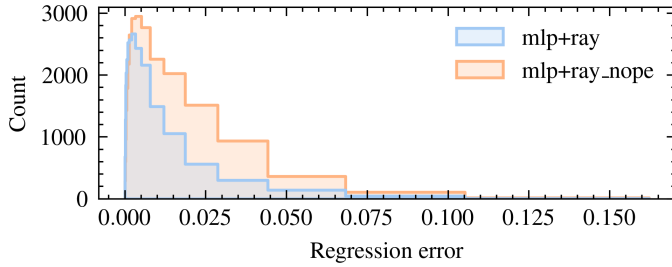


Fig. 10. Histogram of regression errors of MLP with/without positional encoding

using a popular deep-learning framework and optimized via gradient descent. The experiments conducted on real-world data validated the effectiveness of the proposed method and showed significant improvements in the estimation of extrinsic calibration parameters.

REFERENCES

- [1] D. Barnes, M. Gadd, P. Murcutt, P. Newman, and I. Posner, "The oxford radar RobotCar dataset: A radar extension to the oxford RobotCar dataset," pp. 6433–6438, ISSN: 2577-087X.
- [2] K. Burnett, D. J. Yoon, A. P. Schoellig, and T. D. Barfoot, "Radar odometry combining probabilistic estimation and unsupervised feature learning."
- [3] D. Barnes and I. Posner, "Under the radar: Learning to predict robust keypoints for odometry estimation and metric localisation in radar."
- [4] K. Burnett, A. P. Schoellig, and T. D. Barfoot, "Do we need to compensate for motion distortion and doppler effects in spinning radar navigation?" pp. 771–778, conference Name: IEEE Robotics and Automation Letters.
- [5] G. Kim, S. Choi, and A. Kim, "Scan context++: Structural place recognition robust to rotation and lateral variations in urban environments," vol. 38, no. 3, pp. 1856–1874, conference Name: IEEE Transactions on Robotics.
- [6] G. Kim and A. Kim, "Scan context: Egocentric spatial descriptor for place recognition within 3d point cloud map," in *2018 IEEE/RSJ International Conference on Intelligent Robots and Systems (IROS)*, pp. 4802–4809, ISSN: 2153-0866.
- [7] A. Ouaknine, A. Newson, P. Pérez, F. Tupin, and J. Rebut, "Multi-view radar semantic segmentation," pp. 15 671–15 680.
- [8] R. Prophet, G. Li, C. Sturm, and M. Vossiek, "Semantic segmentation on automotive radar maps," in *2019 IEEE Intelligent Vehicles Symposium (IV)*, pp. 756–763, ISSN: 2642-7214.
- [9] J. Rebut, A. Ouaknine, W. Malik, and P. Pérez, "Raw high-definition radar for multi-task learning," pp. 17 021–17 030.
- [10] P. Kaul, D. de Martini, M. Gadd, and P. Newman, "RSS-net: Weakly-supervised multi-class semantic segmentation with FMCW radar," in *2020 IEEE Intelligent Vehicles Symposium (IV)*, pp. 431–436, ISSN: 2642-7214.
- [11] Y. Zhou, L. Liu, H. Zhao, M. López-Benítez, L. Yu, and Y. Yue, "Towards deep radar perception for autonomous driving: Datasets, methods, and challenges," vol. 22, no. 11, p. 4208.
- [12] K. Burnett, D. J. Yoon, Y. Wu, A. Z. Li, H. Zhang, S. Lu, J. Qian, W.-K. Tseng, A. Lambert, K. Y. K. Leung, A. P. Schoellig, and T. D. Barfoot, "Boreas: A multi-season autonomous driving dataset."
- [13] A. Ouaknine, A. Newson, J. Rebut, F. Tupin, and P. Pérez, "CARRADA dataset: Camera and automotive radar with range-angle-doppler annotations."
- [14] A. Sengupta, A. Yoshizawa, and S. Cao, "Automatic radar-camera dataset generation for sensor-fusion applications," vol. 7, no. 2, pp. 2875–2882, conference Name: IEEE Robotics and Automation Letters.
- [15] W. Wang, S. Nobuhara, R. Nakamura, and K. Sakurada, "SOIC: Semantic online initialization and calibration for LiDAR and camera."
- [16] P. Jiang, P. Osteen, and S. Saripalli, "SemCal: Semantic LiDAR-camera calibration using neural mutual information estimator," in *2021 IEEE International Conference on Multisensor Fusion and Integration for Intelligent Systems (MFI)*, pp. 1–7.
- [17] X. Lv, B. Wang, Z. Dou, D. Ye, and S. Wang, "LCCNet: LiDAR and camera self-calibration using cost volume network," pp. 2894–2901.
- [18] G. Zhao, J. Hu, S. You, and C.-C. J. Kuo, "CalibDNN: multimodal sensor calibration for perception using deep neural networks," in *Signal Processing, Sensor/Information Fusion, and Target Recognition XXX*, I. Kadar, E. P. Blasch, and L. L. Grewe, Eds., vol. 11756. SPIE, pp. 324 – 335, backup Publisher: International Society for Optics and Photonics.
- [19] J. Peršić, I. Marković, and I. Petrović, "Extrinsic 6dof calibration of a radar–LiDAR–camera system enhanced by radar cross section estimates evaluation," vol. 114, pp. 217–230.
- [20] B. Mildenhall, P. P. Srinivasan, M. Tancik, J. T. Barron, R. Ramamoorthi, and R. Ng, "NeRF: Representing scenes as neural radiance fields for view synthesis," eprint: 2003.08934.
- [21] C.-H. Lin, W.-C. Ma, A. Torralba, and S. Lucey, "BARF: Bundle-adjusting neural radiance fields," pp. 5741–5751.
- [22] G. El Natour, O. Ait Aider, R. Rouveure, F. Berry, and P. Faure, "Radar and vision sensors calibration for outdoor 3d reconstruction," in *2015 IEEE International Conference on Robotics and Automation (ICRA)*, pp. 2084–2089, ISSN: 1050-4729.
- [23] J. Peršić, I. Marković, and I. Petrović, "Extrinsic 6dof calibration of 3d LiDAR and radar," in *2017 European Conference on Mobile Robots (ECMR)*, pp. 1–6.
- [24] J. Domhof, J. F. Kooij, and D. M. Gavrila, "An extrinsic calibration tool for radar, camera and lidar," in *2019 International Conference on Robotics and Automation (ICRA)*, pp. 8107–8113, ISSN: 2577-087X.
- [25] K. Burnett, "radar_to_lidar_calib," original-date: 2020-10-23T17:41:38Z. [Online]. Available: https://github.com/keen-an-burnett/radar_to_lidar_calib
- [26] G. Yan, L. Zhuochun, C. Wang, C. Shi, P. Wei, X. Cai, T. Ma, Z. Liu, Z. Zhong, Y. Liu, M. Zhao, Z. Ma, and Y. Li, "OpenCalib: A multi-sensor calibration toolbox for autonomous driving."
- [27] P. Jiang and S. Saripalli, "Contrastive learning of features between images and LiDAR," in *2022 IEEE 18th International Conference on Automation Science and Engineering (CASE)*, pp. 411–417, ISSN: 2161-8089.
- [28] Y. Pan, Y. Kompis, L. Bartolomei, R. Mascaro, C. Stachniss, and M. Chli, "Voxfield: Non-projective signed distance fields for online planning and 3d reconstruction," accepted: 2022-07-28T14:17:02Z.
- [29] R. B. Rusu, N. Blodow, and M. Beetz, "Fast point feature histograms (FPFH) for 3d registration," in *2009 IEEE International Conference on Robotics and Automation*, pp. 3212–3217, ISSN: 1050-4729.
- [30] A. Paszke, S. Gross, F. Massa, A. Lerer, J. Bradbury, G. Chanan, T. Killeen, Z. Lin, N. Gimelshein, L. Antiga, A. Desmaison, A. Köpf, E. Yang, Z. DeVito, M. Raison, A. Tejani, S. Chilamkurthy, B. Steiner, L. Fang, J. Bai, and S. Chintala, "PyTorch: An imperative style, high-performance deep learning library."